Remote THz Wave Sensing in Ambient Atmosphere

J.M. Dai, X.F. Lu, J. Liu, I.C. Ho, N. Karpowicz, and X.-C. Zhang*
Center for Terahertz Research
CII 9009, Rensselaer Polytechnic Institute, Troy, NY 12180-3590 USA
Phone/Fax: (518) 276-3079/3292; web: http://www.rpi.edu/terahertz/
*Email: zhangxc@rpi.edu

Abstract: Historically, THz technologies were mainly used within the astronomy community for studying cosmic far-infrared radiation background, and by the laser fusion community for the diagnostics of plasmas. Since the first demonstration of THz wave time-domain spectroscopy in the late 80's, there has been a series of significant advances (particularly in recent years) as more intense THz sources and more sensitive detectors provide new opportunities for understanding the basic science in the THz frequency range. Now, the region of the electromagnetic spectrum from 0.3 to 10 *THz* (1 *mm* – 30 μm wavelength) is a frontier for research in physics, chemistry, biology, materials science and medicine. Ambient air, when excited with intense femtosecond laser beams, exhibits a remarkable ability to generate and detect pulsed THz waves through an optical nonlinear process. The use of air (or selected gases) as a broadband THz wave emitter and THz wave sensor provides superior bandwidth (0.5 - 20 *THz* at 10% bandwidth), sensitivity (heterodyne), resolution (<MHz), and the standoff sensing capability in atmosphere which was heretofore considered impossible due to water vapor attenuation. However, research into the basic science and engineering of THz waves in laser-induced air plasma, especially the application of wide-band and high-field THz waves with standoff capability, is just beginning. Our proposed instrumentation development explores this new area, with an emphasis on broadband spectroscopy, remote sensing and nonlinear effect.

Keywords: Terahertz generation, THz detection, THz spectroscopy, nonlinear optics, air photonics, remote sensing

doi: 10.11906/TST.131-143.2009.12.14

1. Introduction

Recent, significant advances in THz science and technology have opened up a range of potential research opportunities. Applications including label-free DNA genetic analysis, cellular level imaging, chemical/biological sensing, explosives detection, tomographic imaging, and non-destructive testing have thrust THz research from relative obscurity to new heights. This THz wave air-plasma photonics system, with an all-air-based emitter and sensor, does not suffer from semiconductor phonon absorption or emitter geometry features which currently limit conventional THz methods. As a result, the system is limited only by the laser pulse bandwidth, and demonstrates a bandwidth that is unachievable by many conventional pulsed THz wave sensors.

2. THz Air-Breakdown-Coherent-Detection (THz-ABCD)

The fundamental research of THz waves will have an impact in many scientific areas, beyond its historical uses in the astronomy and the laser fusion communities; [1-5] and the technology it develops will be applied in advanced photonic laboratories around the world [6-8]. Our THz wave air-plasma photonics system, [9,10] which differentiates itself from the most THz time-domain spectrometer systems, [11-15] uses ambient air and selected gases for both generation and detection of broadband THz waves. Ambient air and different selected gases,

excited by an intense femtosecond laser beam, exhibit a remarkable ability to generate and detect pulsed THz waves through a high order nonlinear effect. The use of gases as pulsed THz wave emitters and THz wave sensors provides superior bandwidth, sensitivity (heterodyne method), and resolution (<MHz) which were heretofore considered impossible [16]. Fig.1a illustrates this all-optical process for the generation and detection of THz waves by using an air emitter and sensor.

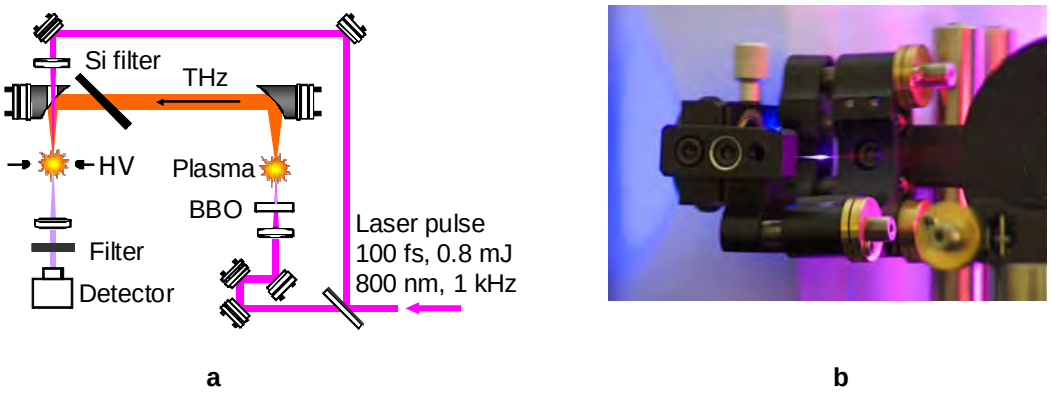

Fig.1 a. Schematic diagram of the THz-ABCD design concept. A laser pulse is focused through a beta barium borate (BBO) crystal to generate its second harmonic beam. The mixed fundamental and its second harmonic beams generate a THz wave at the ionizing plasma spot. The THz and optical beams are recombined at the detection region. An electric bias (HV) is applied to the detection region, supplying a second harmonic local oscillator for coherent detection. b. Laser-induced air plasma (center bright line) emits an intense THz field.

A Ti:Sapphire regenerative amplifier (~800 μJ, 100 *fs* and 1 *kHz* repetition rate with a central wavelength at 800 *nm*) is used as a laser source. The laser beam is focused through a 100-*nm* thick type-I beta barium borate (BBO) crystal to generate its second harmonic beam. The mixed fundamental (ω) and its second harmonic beams (2ω) generate a THz wave at the ionizing plasma spot. An electric bias field is applied to the detection region, supplying a second harmonic local oscillator for coherent detection via a photomultiplier detector [17]. The laser-induced air plasma, shown as a bright line in Fig.1b, emits a very intense, highly directional, ultra-broadband THz field. Similar to the widely used generation and detection of THz waves in electro-optic crystals by second order optical nonlinearity, the THz waves can be detected by the third-order optical nonlinearity. Fig.2a and 4b plot typical temporal THz signal and its spectrum using nitrogen gas as THz wave emitter and sensor with 100 *fs* laser pulse, and Fig. 2c and 4d plot temporal THz signal and its spectrum using 32 *fs* laser pulse duration, respectively. The dips at 18.3 and 22 *THz* are due to two phonon absorption from silicon filter in THz beam path.

3. Using Air as THz Wave Emitter

Air or selected gases, when excited with a dual-color femtosecond laser beam (ω and 2ω), exhibit a remarkable ability to generate and detect pulsed THz waves through optical nonlinear effects. This effect was first reported by Cook and Hochstrasser [12] and treated through perturbation theory as a four-wave mixing process, and later treated semi-classically by Kim [18] and Thomson, [19] assigning the generation process to the formation of a current or polarization of the ionizing electrons, respectively. We treat the ionization process quantum-mechanically by

numerically solving the time-dependent Schrödinger equation, [20] which accurately describes the formation and acceleration of the relevant electron wave packets. Once formed, the wave packets freely propagate into the surrounding medium and eventually collide with a neighboring atom, losing coherence with the original laser-atom system. This process is illustrated in Fig.3, with both schematic diagrams and calculated wavefunctions.

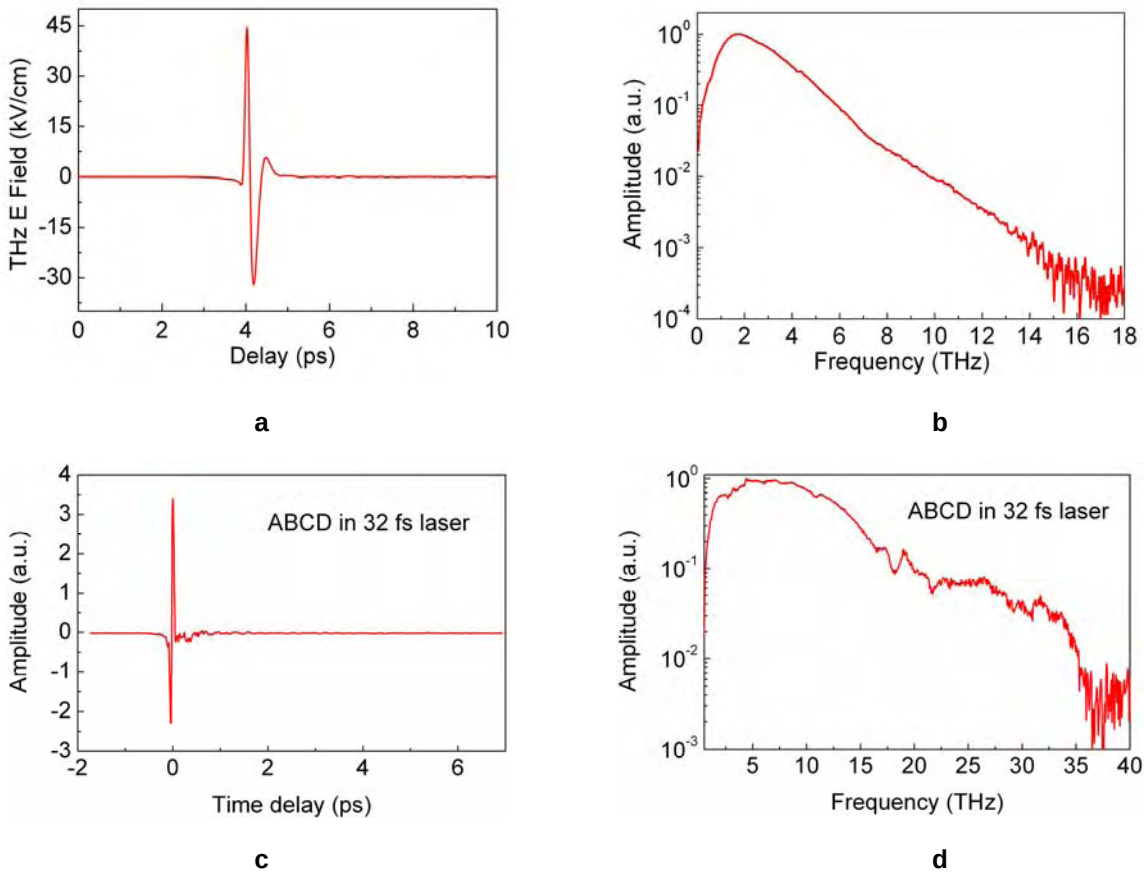

Fig.2 a. Time-resolved THz signal generated and detected using dry nitrogen gas. The probe beam has energy of 85 *J* and a pulse duration of 100 *fs*. b. Log scale plot of the spectrum. Its bandwidth covers a major part of the THz gap (0.1 *THz* to 10 *THz*). c Time-resolved THz signal generated and detected using dry nitrogen gas. The laser pulse duration is 33 *fs*. d Log scale plot of the spectrum. Its 10% bandwidth covers a major part of the THz gap (0.1 *THz* to 10 *THz*).

The interaction emits THz radiation in two steps: first, THz photons are emitted due to the acceleration of the wave packets, which is given a net dipole moment through the asymmetry introduced by the two-color field. Next, when the wave packets collide with the neighboring atoms, they emit bremsstrahlung. Although the scattering time τ for each wave packet is random, the component of the velocity change along the direction of the laser polarization will be anti-parallel to that of the wave packet propagation, resulting in coherent build-up of the resulting radiation at frequencies smaller than the mean of $1/(2\tau)$.

Changing the phase between the fundamental and second harmonic pulses results in a dramatic change in the angular distribution of the wave packets [21]. At this intensity, when the phase is near multiples of π, the distribution of the wave packets along the laser polarization axis is

strongly asymmetric, but it is almost symmetric near odd multiples of π/2. This is demonstrated at the bottom of Fig.3, where the probability densities for the phases corresponding to maximal and minimal THz generation are shown.

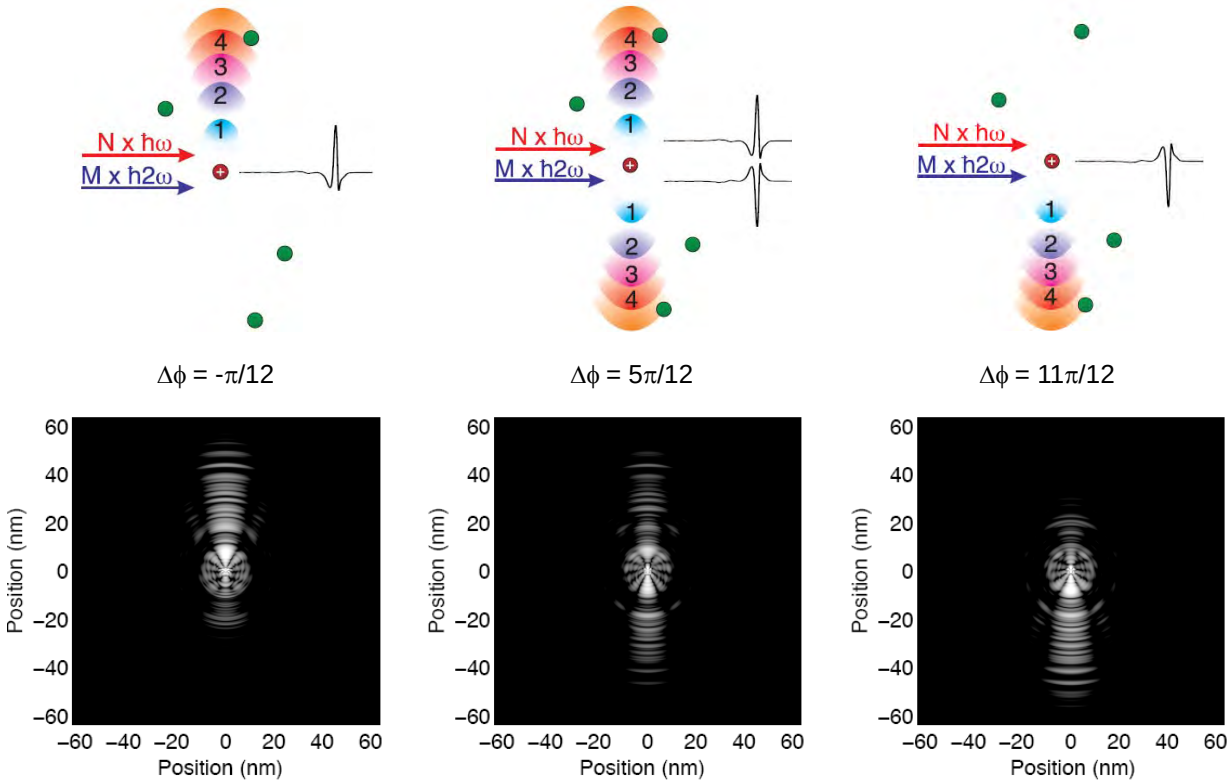

Fig. 3 Top Illustration of the THz radiation process. High intensity laser light, composed of fundamental and second harmonic frequency components (ω and 2ω), interacts with the atom, resulting in tunnel ionization. Some of the wave packets formed in the ionization process are accelerated away from the atom, emitting THz radiation. The wave packets propagate away from the parent atom with quantized velocities, where the numbers indicate the number of photon energy quanta given to each wave packet. They then interact with their surroundings (in this case, a neutral atom) and emit bremsstrahlung, which adds coherently, resulting in a second source of terahertz radiation. Bottom Calculated electron density distributions by numerically solving the time-dependent Schrödinger equation for argon subjected to an intense optical field composed of fundamental and second harmonic pulses with three phase differences, resulting in maximal, minimal and maximal asymmetry in three phases (-π/12, 5π/12, 11π/12)respectively. Left and right diagrams show asymmetric electron wave packages, with net THz fields of opposite polarity, while the center diagram shows the symmetric distribution of electron wave package which radiates symmetric THz fields (same amplitude but opposite polarity) but are cancelled at far field.

By adjusting the timing between the ω and 2ω beam paths by as much as 0.67 *fs* ($\Delta\varphi = \pi$) using the quartz plate (phase plate), [12, 22] opposite polarizations of THz wave are measured, as shown in Fig. 4a. Fig. 4b plots the temporal interference pattern of the THz field versus time delay between ω and 2ω; Fig. 4c is a plot with expanded scale. The step of delay in Fig. 4c is 35 attoseconds [22].

With a newly constructed phase compensator, the relative phase between the 800 and 400 *nm* pulses can be precisely controlled below a femtosecond which has far better stability than our requirement for standoff generation. The new design of the THz air-plasma photonic system

allows us to achieve stable THz wave generation and detection over 100 meters (even one kilometer) [22].

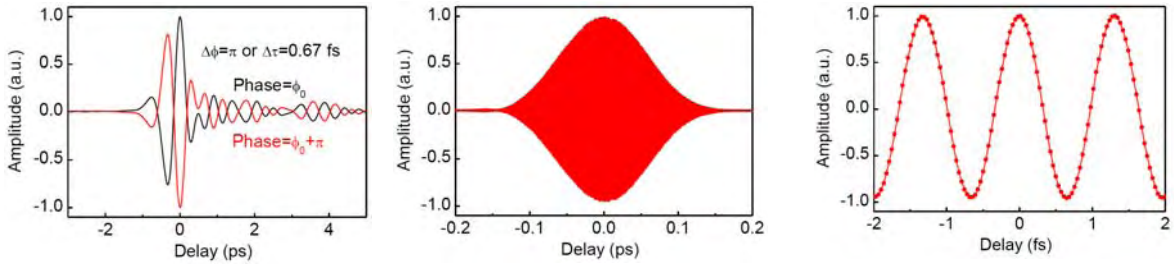

a **b** **c**

Fig. 4 a. THz waveform flips when the phase difference between the ω and 2ω beam is changed by π. This corresponds to about 667 attoseconds additional time delay. b. Measured peak THz signal versus time delay (0.4 *ps*) between ω and 2ω; c. Same data shown in expanded scale (4 *fs*). Each delay step is 35 attoseconds; SNR > 1000:1 of THz field is achieved.

4. Using Biased Air or Selected Gas as THz Heterodyne Sensor

The basic detection principle utilized gas to sense the pulsed THz waves as a measurement of the THz-field-induced optical second harmonic generation through a third-order nonlinear process [23,24]. Here, by focusing the THz pulse with the probe beam fundamental (ω) pulse, an optical field at the second harmonic frequency (2ω) is formed such that [25]

$$E_{2\omega}(t) \propto \chi^{(3)}_{xxxx} E_{THz}(t-\tau) E_{\omega}(t) E_{\omega}(t) \quad (1)$$

Where $E_{2\omega}$, E_{ω}, and E_{THz} are the electric field amplitudes of the 2ω, ω, and THz waves, respectively, and (3) is the third-order susceptibility of the gas.

Since the $E_{2\omega}(t) \propto E_{THz}(t-\tau)\ E_{\omega}(t)\ E_{\omega}(t)$, it follows that the intensity of the measured second-harmonic signal by the photon-multiplier-tube (PMT) is proportional to the intensity of the THz wave: $I_{2\omega}(t) \propto I_{THz}(t-\tau)$, the measurement predicted in Eqn. (1) is incoherent, therefore the phase information is lost.[10]

One of the most valuable properties of THz time-domain spectroscopy is coherent detection. If the air sensor detection is incoherent, then its applications will be very limited. By introducing an external bias to the optical focus, a bias-field-induced second harmonic pulse, with field amplitude designated by $E^{LO}_{2\omega}$, is generated. This additional second harmonic pulse mixes with the THz-field-induced second harmonic pulse $E^{THz}_{2\omega}$. The carrier-envelope phase relative to that of the THz-field-induced second harmonic pulse can be changed from 0 to π by changing the direction of the bias field, and the total second-harmonic intensity in terms of the time-dependent electric fields has the form:

$$I_{2\omega} \propto \langle E_{2\omega}{}^2 \rangle = \langle (E^{THz}_{2\omega} + E^{LO}_{2\omega})^2 \rangle = \langle E^{THz\ 2}_{2\omega} \rangle \pm 2 \langle E^{THz}_{2\omega} E^{LO}_{2\omega} \rangle + \langle E^{LO\ 2}_{2\omega} \rangle \quad (2)$$

Since the difference in carrier phase between $E_{2\omega}^{THz}$ and $E_{2\omega}^{LO}$ is either 0 or π, the cross term has a constant value (but alternating sign), and thus the time-averaging notation can be dropped. The THz-field-induced second harmonic $E_{2\omega}^{THz}$ and the AC-bias-induced second harmonic $E_{2\omega}^{LO}$ can be written as:

$$E_{2\omega}^{THz}(\tau) \propto \chi^{(3)} E_{\omega}(t) E_{\omega}(t) E_{THz}(t-\tau) = \chi^{(3)} I_{\omega}(t) E_{THz}(t-\tau) \quad (3)$$

$$E_{2\omega}^{LO}(t) \propto \chi^{(3)} E_{\omega}(t) E_{\omega}(t) E_{bias} = \chi^{(3)} I_{\omega}(t) E_{bias} \quad (4)$$

Where E_{bias} is the bias applied on the sensor gas. Using Eqns. (3) and (4), Eqn. (2) can be written as:

$$I_{2\omega}(\tau) \propto (\chi^{(3)} I_{\omega}(t))^2 [(E_{THz}(t-\tau))^2 \pm 2 E_{bias} E_{THz}(t-\tau) + (E_{bias})^2]. \quad (5)$$

Due to the phase modulation of the bias-induced second harmonic, the process can be interpreted in terms of heterodyne detection. Only the cross term is present at the modulation frequency, while the other terms exist only on the laser repetition rate and its even harmonics, and thus lock-in amplification easily isolates the signal proportional to E_{THz}. The measured second harmonic intensity will be:

$$I_{2\omega}(\tau) \propto 2 [\chi^{(3)} I_{\omega}(t)]^2 E_{bias} E_{THz}(t-\tau) \quad (6)$$

Eqn. (6) is the most important result for detection. The linearity of $I_{2\omega}$ versus E_{bias} indicates heterodyne detection when E_{bias} is treated as a local oscillator. The field-induced-second-harmonic signal $I_{2\omega}$ is quadratically proportional to $\chi^{(3)}$, $I_{\omega}(t)$, and linearly proportional to E_{bias}, $E_{THz}(t-\tau)$.

To test the validity of Eqn. (6), Fig. 7a plots detected THz field versus (3), normalized by the value of nitrogen $\chi^{(3)}(N_2)$ in six saturated Alkane (C_nH_{2n+2}) gases. C_6H_{14} is over 24 times more sensitive than the use of N_2 or air. The signal-to-noise ratio (SNR) increases with increased $I_{\omega}(t)$ until the probe energy reaches the plasma threshold. Fig. 7b shows THz field versus biased field with air, Xe, and SF_6 under the same pressure [26, 27]. Increasing the bias field leads to an increased signal-to-noise ratio, but once the signal is significantly higher than the dark noise of the detector, the SNR is limited by the laser noise.

Eqn. (6) could be the key to optimizing THz wave detection in gases. First of all, Eqn. (6) shows that the field-induced-second-harmonic signal $I_{2\omega}$ is quadratically proportional to $\chi^{(3)}$ and $I_{\omega}(t)$. Therefore, to use gases with a large value $\chi^{(3)}$ or at higher gas pressure (since the effective $\chi^{(3)}$ is proportional to the number of molecules at low pressure), or with higher probe pulse energy are the best choices. We will test conjugated hydrocarbons which contain alternating single and double bonds. These conjugated hydrocarbons (such as C_4H_6 and C_5H_8) can possess an extremely large nonlinear optical response due to their π bonds which tend to be delocalized and respond more freely to an applied optical field.

Second, Eqn. (6) shows that $I_{2\omega}$ is linearly proportional to E_{bias}, an equation of typical heterodyne detection. As SF_6 has a static breakdown threshold (300 *kV/cm*) 10 times higher than that of air (30 *kV/cm*), its experimental setup could use a higher bias field Ebias (or local

oscillator strength). Eqn. (6) also provides a method for estimating the absolute THz field strength E_{THz}. Since the field E_{bias} can be measured directly, a comparison between the second harmonic intensity induced by the bias E_{bias} and the THz field E_{THz} yields the average THz amplitude in the detection region. The measured THz field is between 50 *kV/cm* and 200 *kV/cm* with 600-μJ input pulse energy.

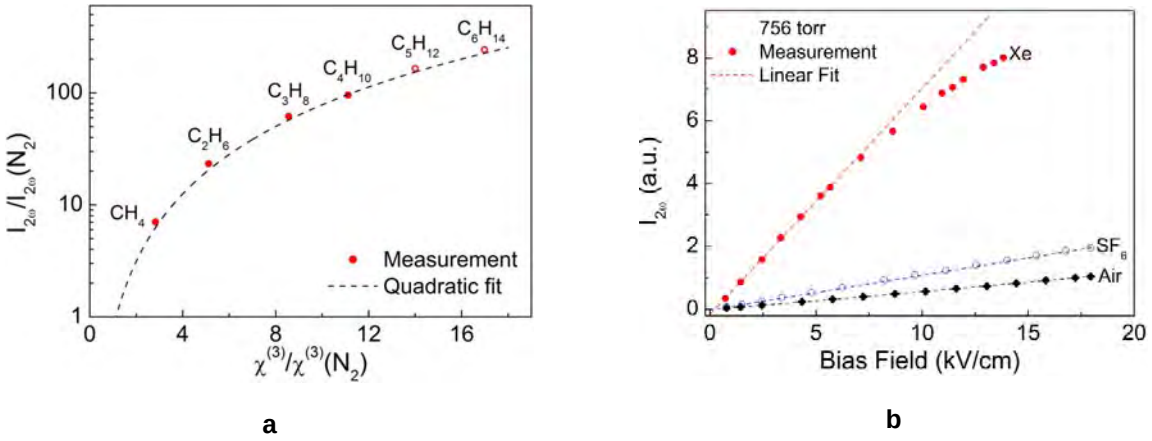

Fig. 5 Experimental evidence for validation of Eqn. (6). a. Measured THz field versus normalized $\chi^{(3)}$ from saturated Alkane (C_nH_{2n+2}) gases. Using C_6H_{12} as a sensor is 243 times more sensitive than the use of N2 or air. $\chi^{(3)}$ values for C_5H_{12} and C_6H_{14} are calibrated by using known C_3H_8 $\chi^{(3)}$ value in the THz-ABCD system. b. Plots of $E_{THz} \propto I_{2\omega}(\tau) \propto E_{bias}$ in air, SF_6, and Xe. Linearity of the field dependence indicates purely coherent detection.

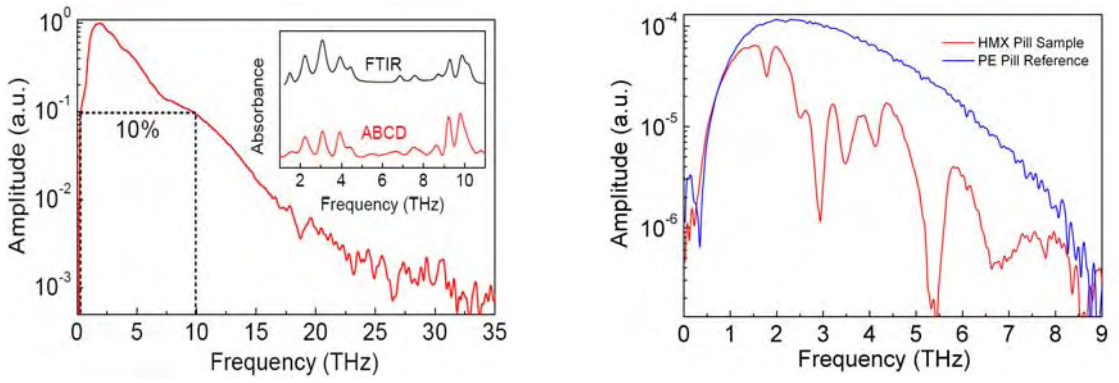

Fig. 6 a. Spectrum of THz-ABCD using dry nitrogen gas as THz wave emitter and sensor. The features in the vicinity of 18.5 *THz* are consistent with the two photon and carbon impurity absorption of the silicon wafer used as a low-pass filter. Inset: Spectra of a 2-2' biphenol sample taken using both the time-domain system and an FTIR spectrometer. b. HMX spectrum (red curve) with a reference spectrum (blue curve) measured by our THz-ABCD.

Since the generation and detection of the THz waves occurs in a gas, the spectrum of the THz time-domain spectrometer is almost solely limited by the properties of the laser pulse. Fig. 8a shows the measured spectrum using dry nitrogen gas as the THz wave emitter and sensor gas. The broad spectral range and heterodyne detection capability allow spectroscopic measurements

across the full THz range. The inset plot in Fig. 8a shows the spectrum of a 2-2' biphenol sample, taken by the THz time-domain system and by a traditional FTIR spectrometer (Bruker). While FTIR is primarily limited to linear spectroscopy, our proposed instrument will provide versatility in bandwidth coverage spanning mm-wave to far-infrared and unlocking the capability for both linear and nonlinear spectroscopy. Fig. 8b plots spectrum of an explosive (HMX) measured by our THz-ABCD with the spectral range to 8 *THz*.

5. Remote Sensing

The proposed THz wave air photonics approach, in contrast to nearly all other THz wave sensing methods, transmits an optical beam in close proximity to the target rather than sending a THz wave in the air. This allows us to sense a target at a greater distance with a phase compensator arrangement which is shown in Fig. 6a. We have achieved 10.5 meters of THz generation with a 0.6 *mJ* laser, the measured waveform of which is shown in Fig. 6b. Remote THz wave generation (>100 meters) is feasible [22]. however, it is very challenging. Backward radiation of THz, THz-field-induced fluorescence, higher harmonics from air (or plasma) with focused optical probe beam will be systematically studied. It is possible that the backward radiation could provide an alternative method to remotely detect THz waves. We will also study the use of an optical phase modulator before the pre-chirp generation in Fig. 6a to convert one optical pulse to a train of optical pulses, and use this to create a THz pulse train in air. A densely packed THz pulse train is a narrow bandwidth THz wave. Its center frequency and bandwidth is determined by the temporal spacing between pulses and the number of pulses in the train. We will perform THz generation and detection at standoff distance with a new amplified laser (6 *mJ*).

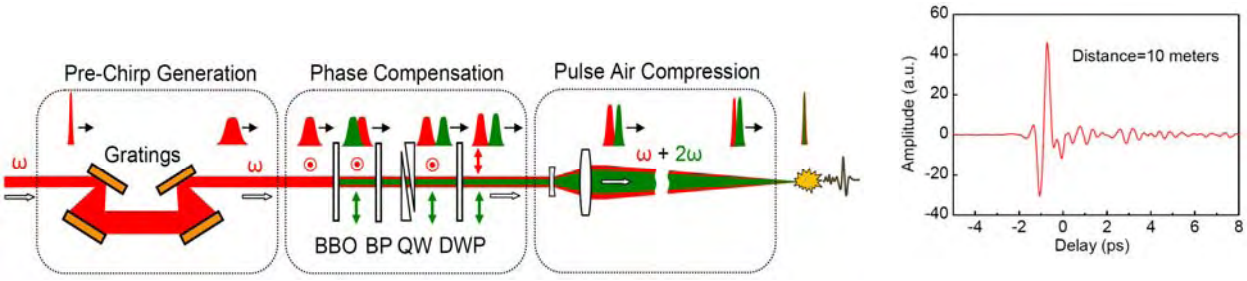

a **b**

Fig. 7 a. Concept of phase compensator for standoff THz wave generation. BP, bi-refringent parallel plate; QW, quartz wedge pair; DWP, dual-band wave plate (half wave retardance at ω and full wave retardance at 2ω). b. Measured THz signal generated 10.5 meters away (from the last optical focusing element to the plasma).

With an upgrade laser system (6 *mJ* <35 *fs*) in this project, it is feasible to achieve THz wave generation greater than 100 meters. However, the challenge is THz wave standoff detection. Here we propose to use THz-field-induced optical fluorescence in plasma. Since the emission of optical fluorescence is in general isotropic, by measuring the intensity change of optical fluorescence from the plasma, a time-resolved THz signal could be measured remotely.

6. THz Radiation-Enhanced-Emission-of-Fluorescence (REEF)

THz air-plasma photonics, especially THz-ABCD, will impact remote sensing. However, sensitivity and selectivity of THz remote detection at standoff distance remains challenging. This is due to the directionality of the THz-field-induced second harmonic wave, as it is very hard to get enough signal from the backward or a sideways direction. It is desirable to find optical phenomena which strongly correlate to the THz signal and can be observed at any angle (isotropic) to eliminate the limitation of collection directionality [28].

Here we introduce a new approach to tackle this long existing challenge. This method is time-resolved broadband remote sensing using THz Radiation Enhanced Emission of Fluorescence (THz REEF). Instead of collecting and measuring the scattered or reflected THz wave far away from the standoff target, we detect the THz signal directly at standoff distance by observing the THz wave enhanced fluorescence emission of air molecules (mainly nitrogen lines). Specifically, air-plasma (or plasma-filament) is formed remotely by focusing an Infrared pulse at a distance of tens of meters up to hundreds or even thousands of meters. The fluorescence emission of photo-excited air molecules in plasma is used as a remote sensor that is able to accurately resolve the THz temporal waveform. Thus THz spectroscopic fingerprint information of the standoff target could be carried back to the operator via a fluorescence signal with a wavelength of 300-450 *nm*. Unlike other methods, this remote sensing method is not limited by THz absorption by moisture due to the atmospheric transparency in this wavelength range.

The schematic of time-resolved, broadband, THz remote sensing using REEF in plasma-filament is illustrated in Fig. 8a. When the THz pulse and IR pulse are spatially and temporally overlapped, the THz electric field would enhance plasma fluorescence emission through a nonlinear electronic disturbance process such as electron acceleration, electron-ion collision, molecule ionization, molecule excitation and etc. The naked eye cannot see the change of fluorescence intensity when a THz field is applied on the plasma. However, more than 60% fluorescence intensity enhancement is observed between 300 to 400 *nm* in the ultraviolet range.

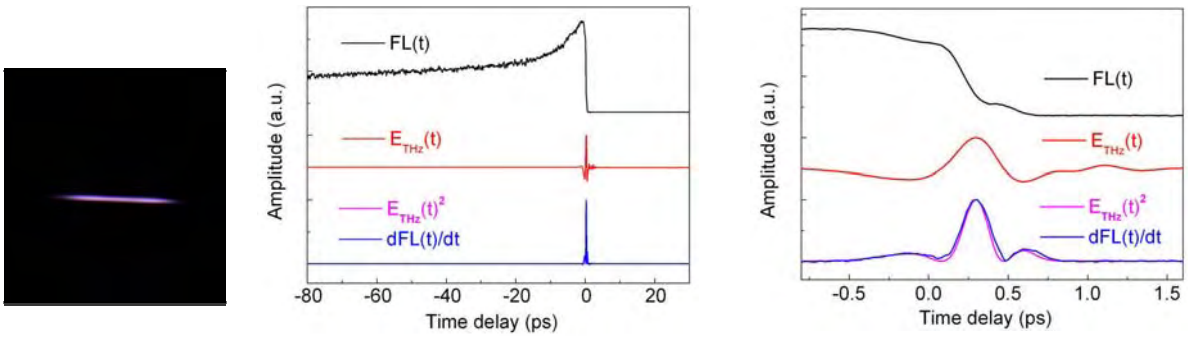

Fig.8 a. THz radiation applied on the plasma-filament (about 1 *cm* long). The nitrogen fluorescence intensity linearly increases with THz energy. b. The temporal correlation of THz-enhanced-fluorescence (top), THz electric field (middle), derivative of THz-enhanced-fluorescence (blue, bottom) and THz intensity (magenta, bottom) in an over 100 *ps* window. The time delay is the relative timing between THz pulse and optical pulse. c. The temporal correlation at a smaller temporal window (about 2.3 *ps*). From the two overlapping bottom curves, excellent agreement between $[E_{THz}(t)]^2$ and $d(FL)/dt_d$ is observed.

In our preliminary study, we investigated the temporal correlation between the enhancement of fluorescence intensity FL) and THz field (E_{THz}), as shown in Fig. 10b and 10c. Their relation can be depicted as Eqn. (7),

$$(FL(t_d)) \propto \int_{t_d}^{\infty} [\, E_{THz}(t) \,]^2 \; dt \tag{7}$$

By mapping out the time-resolved THz-induced-fluorescence emission intensity $FL(t_d)$, the THz intensity can be retrieved by Eqn. (8):

$$[E_{THz}(t)\,]^2 \propto d(FL)/dt_d \tag{8}$$

This equation says that the THz signal (intensity) is proportional to the first time-derivative of fluorescence emission intensity. The emission intensity detection, in general, is not coherent. However, similar to our previous THz-ABCD demonstration, it is possible to achieve coherent detection by applying an additional electric field on plasma as the local oscillator. In this heterodyne approach, both amplitude and phase of the THz field through the detection of TEF are measured simultaneously.

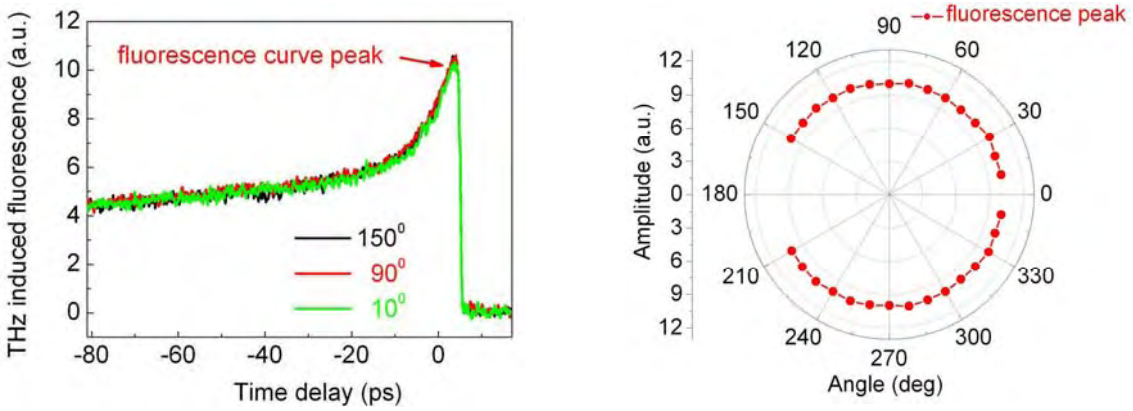

Fig.9 a. Time-resolved THz-enhanced-fluorescence signal (including falling edge in longer time scale) when collection angle is 10^0 (forward), 90^0 (sideward), and 150^0 (backward), respectively. b. The measured angular distribution of fluorescence curve peak. Isotropic emission of enhanced fluorescence is confirmed.

Fig.9a plots the time-resolved THz-enhanced-fluorescence measured at three collection angles. Nearly identical waveforms were obtained at forward, sideward and backward directions. This isotropic nature of TEF, plotted in a Smith Chart shown in Fig. 11b, is inherited from the isotropic nature of fluorescence itself. The multi-exponential decay process of the THz-enhanced-fluorescence signal was also observed. It reveals fundamental physics processes involved in THz sensing, including plasma lifetime elongation, excited states internal conversion and etc. A more comprehensive study of TEF would be needed, not only to gain physical insight into the nature of ps scale dynamic control of fluorescence emission, but also to greatly assist future development of THz remote sensing. In all, with its capability of ultrafast dynamic control, remote sensing and non-invasive detection, TEF is a very promising technique for disciplinary applications of physics, chemistry, bio-medical, remote hazardous gas/liquid/solid detection, pollution control and etc.

Besides its nearly loss-free, long distance propagation in air, another attractive merit of THz remote sensing using THz-enhanced-fluorescence is that its emission profile is isotropic. This would enable the operator to detect the THz signal remotely either backward/sideway or in any direction which is crucial when forward detection is not feasible in a reality case.

7. Conclusions

In the past, majority of THz research was in the linear spectroscopic measurements which use the relative low THz field strength (<1 *kV/cm*) as the source. With new intense THz sources recently developed, more nonlinear THz spectroscopic research (such as on dielectric materials measurement with greater than 100 *kV/cm* or even 1 *MV/cm*), is expected. For comparison, the ambient air electrostatic breakdown field is about 30 *kV/cm*.

The demonstrated THz air photonics has field strength (air emitter), frequency bandwidth (air sensor) and field sensitivity (heterodyne detection) that is not currently available from any commercial company. The authors believe that it could be one of the critical vehicles in the study of THz-plasma dynamic interaction, ultra-broadband spectroscopy, remote sensing, nonlinear phenomena, and other future endeavors [29-33].

Acknowledgement

We gratefully acknowledge support from the United State National Science Foundation, the Defense Threat Reduction Agency, the Office of Naval Research, and the Department of Homeland Security through the DHS-ALERT Center under Award No. 2008-ST-061-ED0001. The views and conclusions contained in this document are those of the authors and should not be interpreted as necessarily representing the official policies, either expressed or implied, of the U.S. Department of Homeland Security.

References

[1] Grischkowsky, D., Keiding, S., Exter, M., and Fattinger, Ch. Far-infrared time-domain spectroscopy with THz beams of dielectrics and semiconductors. *Journal of the Optical Society of America* B 7, 2006 – 2015, (1990).

[2] Cole, B. E., Williams, J. B., King, B. T., Sherwin, M. S., Stanley, C. R. Coherent manipulation of semiconductor quantum bits with terahertz radiation. *Nature* 410, 60 – 63, (2001).

[3] Carr, G. L. Martin, M.C., McKinney, W.R., Jordan, K., Neil, G.R., Williams, G.P. High-power terahertz radiation from relativistic electrons. *Nature* 420, 153 – 156, (2002).

[4] Köhler, R., Tredicucci, A., Beltram, F., Beere, H.E., Linfield, E.H., Davies, A.G., Ritchie, D.A., Iotti, R.C., Rossi, F. Terahertz semiconductor-heterostructure laser. *Nature* 417, 156 – 159, (2002).

[5] Ferguson, B., Zhang, X.-C. Materials for terahertz science and technology. *Nature Materials* 1, 26 – 33, (2002).

[6] Zandonella, C. Terahertz imaging: T-ray specs. *Nature* 424, 721 – 722, (2003).

[7] Kaindl, R. A., Carnahan, M. A., Hägele, D., Lövenich, R., Chemla, D. S. Ultrafast terahertz probes of transient

conducting and insulating phases in an electron-hole gas. *Nature* 423, 734 – 738, (2003).

[8] Wang, K., Mittleman, D.M. Metal wires for terahertz wave guiding. *Nature* 432, 376 – 379, (2004).

[9] Xie, X., Dai, J., and Zhang, X.-C. Coherent control of THz wave generation in ambient air. *Physical Review Letters* 96, 075005, (2006).

[10] Dai, J., Xie, X., and Zhang X.-C. Detection of broadband terahertz waves with a laser-induced plasma in gases. *Physical Review Letters* 97, 103903, (2006).

[11] Hamster, H., Sullivan, A., Gordon, S., White, W., Falcone, R.W. Subpicosecond, electromagnetic pulse from intense laser-plasma interaction. *Physical Review Letters* 71, 2725-2728, (1993);

[12] H. Hamster, A. Sullivan, S. Gordon, and R. W. Falcone, Short-pulse terahertz radiation from high-intensity-laser-produced plasma. *Physical Review E* 49, 671, (1994).

[13] Cook, D.J., Hochstrasser, R.M. Intense terahertz pulses by four-wave rectification in air. *Optics Letters* 25, 1210-1212, (2000).

[14] Tzortzakis, S., Méchain, G., Patalano, G., André, Y.-B., Prade, B., Franco, M., Mysyrowicz, A., Munier, J.-M., Gheudin, M., Beaudin, G., & Encrenaz, P. Coherent subterahertz radiation from femtosecond infrared filaments in air. *Optics Letters* 27, 1944-1946, (2002).

[15] Kress, M., Löffler, T., Eden, S., Thomson, M., & Roskos, H.G. Terahertz-pulse generation by photoionization of air with laser pulses composed of both fundamental and second-harmonic waves. *Optics Letters* 29, 1120-1122, (2004).

[16] T. Löffler, M. Kress, M. Thomson and H.G. Roskos, Efficient terahertz pulse generation in laser-induced gas plasmas, *ACTA PHYSICA POLONICA A* 107, 99, (2005).

[17] T. Bartel, P. et al. Generation of single-cycle THz Transients with high electric-field amplitudes, *Optics Letters* 30, 2805 - 2807, (2005).

[18] Karpowicz, N., Chen, J., Tongue, T., and Zhang, X.-C. Coherent millimeter wave to mid-infrared measurements with continuous bandwidth reaching 40 THz. *Electronics Letters* 44, 544-545, (2008).

[19] Karpowicz, N., Dai, J., Lu, X.F., Zhang, Z.Z., Zhang, C.L., Chen, Y.Q., Yamaguchi, M., Zhao, H.W., Price-Gallagher, M., Johnson, K., Mamer, O., Lesimple, A., Fletcher, C., and Zhang, X.-C. A coherent heterodyne time-domain spectrometer covering entire terahertz "gap". *Applied Physics Letters* 92, 011131, (2008).

[20] Kim, K. Y., Glownia, J. H., Taylor, A. J., and Rodriguez, G. Terahertz emission from ultrafast ionizing air in symmetry-broken laser fields. *Optics Express* 15, 4577 – 4584, (2007).

[21] Thomson, M.D., Kreß, M., Löffler, T., Roskos, H.G. Broadband THz emission from gas plasmas induced by femtosecond pulses: from fundamentals to applications. *Laser & Photonics Reviews* 1, 349-368, (2007).

[22] Karpowicz, N., and Zhang, X.-C. Coherent terahertz echo of tunnel ionization in gases. Submitted to *Physical Review Letters*, (2008).

[23] Schumacher, D.W., Bucksbaum, P.H. Phase dependence of intense-field ionization *Physical Review A* 54, 4271 – 4278, (1996).

[24] Dai, J., and Zhang, X.-C Terahertz wave generation from gas plasma at standoff distances using a phase compensator with attosecond phase-control accuracy. *Applied Physics Letters*, (2009). In press.

[25] Nahata, A., and Heinz, T. F. Detection of freely propagating terahertz radiation by use of optical second-harmonic generation. *Optics Letters* 23, 67-69, (1998).

[26] Cook, D. J., Chen, J. X., Morlino, E. A., Hochstrasser, R. M. Terahertz-field-induced second-harmonic generation measurements of liquid dynamics. *Chemical Physics Letters* 309, 221-228, (1999).

[27] Boyd, R. W., Nonlinear optics, *Academic Press*, Boston, (1992).

[28] Lu, X.F., Karpowicz, N., Chen, Y., and Zhang, X.-C. Systematic study of broadband terahertz gas sensor. *Applied Physics Letters* 93, 261106, (2008).

[29] Lu, X.F., Karpowicz, N., and Zhang, X.-C. Broadband THz detection with selected gases, *JOSA B* 26, A66, (2009).

[30] Liu, J., and Zhang, X.-C. Terahertz radiation enhanced emission of fluorescence from gas plasma, *Phys. Rev. Letts.* ,(2009). In press.

[31] Karpowicz, N., Lu, X.F., and Zhang, X.-C. Terahertz Gas Photonics, topical review paper, *Journal of Modern Optics*, 56, 1137–1150, (2009).

[32] Karpowicz, N., Dai, J.M., and Zhang, X.-C. Recent developments in broadband terahertz spectroscopy, *International journal of high speed electronics and systems*, 18, 1005-1012, (2008).

[33] Dai, J.M., Karpowicz, N., and Zhang, X.-C. Coherent polarization control of terahertz waves generated from two-color laser-induced gas plasma," *Phys. Rev. Lett.* 103, 023001, (2009).

[34] Karpowicz, N., Lu, X.F., and Zhang, X.-C. The role of tunnel ionization in THz gas photonics, *Laser Physics*, Vol. 19, No. 8, pp. 1535–1539, (2009).

[35] Dai, J.M., Karpowicz, N., and Zhang, X.-C. Optically Manipulating Terahertz Wave Polarization in Two-Color Laser-Induced Gas Plasma, *Optics in 2009, OPN*, (2009). In press.